SAND80-8856
Unlimited Release

Corrosion of 304SS by Molten $NaNO_3$-KNO_3 in a Thermal Convection Loop

R. W. Bradshaw

Prepared by Sandia Laboratories, Albuquerque, New Mexico 87115
and Livermore, California 94550 for the United States Department
of Energy under Contract DE-AC04-76DP00789.

Printed December 1980

Sandia Laboratories
energy report

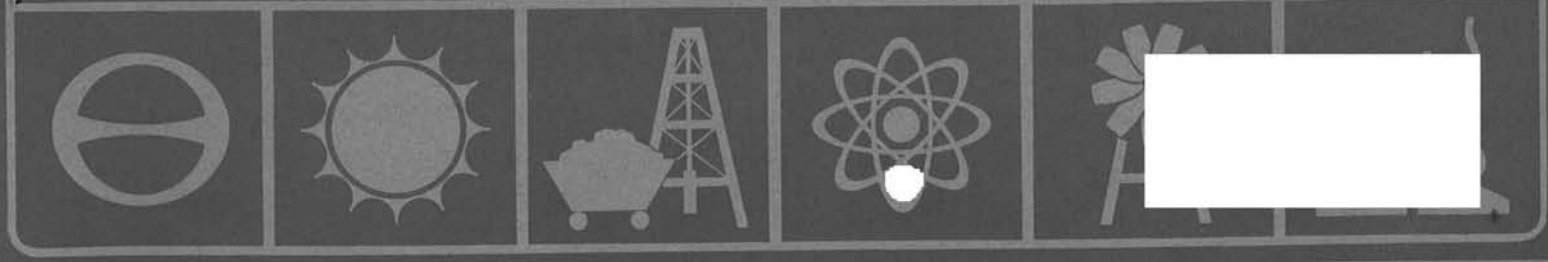

Issued by Sandia National Laboratories, operated for the United States Department of Energy by Sandia Corporation.

NOTICE

Printed in the United States of America
Available from
National Technical Information Service
U. S. Department of Commerce
5285 Port Royal Road
Springfield, VA 22161
Price: Printed Copy $4.50 ; Microfiche $3.00

SAND80-8856
Unlimited Release
Printed December 1980

CORROSION OF 304SS BY MOLTEN $NaNO_3$-KNO_3 IN A THERMAL CONVECTION LOOP

R. W. Bradshaw
Exploratory Chemistry Division I, 8313
Sandia National Laboratories, Livermore

ABSTRACT

The corrosion behavior of Type 304 stainless steel in molten $NaNO_3$-KNO_3 was studied at temperatures between 600°C and 350°C using thermal convection loops. Corrosion rates were somewhat less than 2.5×10^{-2} mm/year (1 mil/year) at the maximum temperature. Two corrosion processes were observed, formation of oxide scales and depletion of chromium from the alloy. Oxidation products generally consisted of at least two layers, a layer of Fe_3O_4 over an iron-chromium spinel. In addition, a complex oxide was detected which appeared to be a double oxide of iron and, a salt impurity, magnesium. Chromium accumulated as a soluble product in the melt but thermal gradient mass transfer was not observed. Chromium depletion kinetics were approximately parabolic with time suggesting a diffusion controlled process. Autogenous weldments experienced somewhat more corrosion in the heat-affected zone than either the fusion zone or the parent alloy.

CONTENTS

ILLUSTRATIONS

TABLES

Acknowledgments

The following people contributed significantly to this effort.

D. R. Boehme	X-ray diffraction
W. M. Clift	Auger spectroscopy
H. C. Feemster	Chemical analysis
F. W. Hart	Apparatus design and fabrication
A. James	Metallography
C. W. Karfs	Electron microscopy
D. E. Meeker	Chemical analysis
M. J. Nash	Electroplating

CORROSION OF 304SS BY MOLTEN $NaNO_3$-KNO_3 IN A THERMAL CONVECTION LOOP

Introduction

Molten nitrate salts are potentially attractive as working fluids in central solar receivers and as thermal energy storage media in sensible heat systems [1,2]. These applications may be viewed as extensions of industrial uses of molten salts for heat transfer, which have been practiced for many years [3]. A mixture of particular interest is 60 $NaNO_3$-40 KNO_3 (w/o), which offers chemical stability at high temperature, desirable physical properties and low cost and which is the basis for a prototype central solar receiver design [4].

The choice of containment materials for a molten salt system is based on a variety of factors including corrosion resistance, mechanical properties and cost. In a central solar receiver, the maximum temperature expected is 600°C (1110°F) and the working environment is a complex one involving daily cycling of temperature and stress. Alloys which are commonly used in this temperature range include the 300-series stainless steels and Incoloy 800.

Relatively little data has been published concerning corrosion of high temperature alloys in molten nitrates at the temperatures of interest in solar applications. I800 and 316SS have been reported to undergo relatively slow scaling in a molten nitrate mixture at 595°C, resulting in weight gains of a few mg/cm^2 after several thousand hours [4]. In another study, an analysis

of Inconel 600 after 700 hours at 550°C revealed about 5 microns of scaling and about 20 microns of intergranular oxidation [5].

Additional results have been reported concerning corrosion of stainless steels in a related salt mixture consisting of 40 $NaNO_2$-53 KNO_3-7$NaNO_3$ commonly referred to as heat transfer salt (HTS) or HITEC. These studies were limited to 550°C because of decomposition of the salt. At temperatures of 500°C, stainless steels appear to provide good corrosion resistance [6], although an unquantified amount of intergranular oxidation has been reported [7,8]. Some experiments with 316SS and 310SS at 550°C showed corrosion rates less than 1 mil/year and indicated that corrosion produces primarily iron oxides [9]. Intergranular oxidation was not observed in the latter study. 316SS was reported to experience rapid weight reduction at 550°C in convection loop tests with HITEC, resulting in as much as 140 μm/year of metal loss [10].

The data reviewed above are not adequate for the purposes of designing central solar receivers and thermal energy storage systems using molten $NaNO_3$-KNO_3 at 600°C. The work reported here is part of a program to develop the necessary data base concerning the corrosion behavior of high temperature alloys in molten nitrates This report describes the results of corrosion experiments of a representative stainless steel, 304SS, and considers their implications with respect to receiver performance.

Experimental

A thermal convection loop was used as the experimental system in order to simulate the range of temperatures expected in a central solar receiver heat exchanger circuit in a single apparatus. The key feature of a thermal convection loop is that a mass flow can be induced by a thermosiphon which is created by heating one vertical leg and dissipating heat from the other legs of the loop.

The existence of a temperature gradient and mass flow enables the experimenter to observe tendencies for thermal gradient mass transfer as well as study corrosion as a function of temperature. The design and operation of the loop have been described in detail elsewhere [11].

The temperature profile obtained in the loop is plotted in Figure 1. The maximum temperature was 600°C and the minimum was 350°C with gradient of approximately 3°C/cm in the heated leg. Temperature variations were $\pm$ 5°C at a given location although short term variations were occasionally twice that value. The loop operates at steady-state conditions and thus the thermal cycles intrinsic to central solar receivers were not simulated in these experiments.

The chemical compositions of the materials used to fabricate the loop and the removeable coupons are given in Table I. Coupons were polished with 180 grit SiC paper and then cleaned ultrasonically in isopropyl alcohol. No surface preparation was used for the tubing. Autogeneous weldments of coupon stock were produced by gas-tungsten arc welding and contained sections of the parent alloy and fusion and heat-affected zones.

Inserted coupons were suspended from a sample tree at various locations to cover a range of temperatures. They were periodically removed for weighing and metallographic analysis. Specimens were quenched in air, rinsed in an ultrasonically agitated hot water bath, dried and weighed. At the termination of the experiment, the loop was sectioned for metallographic analysis. Metallographic specimens were electroplated with nickel before polishing in order to maintain the integrity of surface scales [12].

In addition to examination of metallic coupons, the melt within the loop was periodically sampled and chemically analyzed. The salt initially charged was a commercially pure mixture of 60 $NaNO_3$-40 KNO_3 (w/o), (Partherm 430 ,

Park Chemical Co., Detroit, MI). Since the loop was allowed to breathe to the atmosphere, some decomposition of NO_3^- to NO_2^- was observed as well as absorption of CO_2 from the atmosphere. Concentrations of NO_2^-, CO_3^{-2} and oxide ion (as OH^-) were determined by titrimetic methods after dissolving quenched melt samples in water [13]. Metallic content was determined by atomic absorption spectroscopy. Additional salt was added only as needed to compensate for periodic withdrawals of 10 gm samples for chemical analysis.

The results of chemical analyses for NO_2^- and $CO_3^=$ appear in Table III. No oxide could be detected by the analytical technique which was sensitive to 5×10^{-4} moles/kg [13]. The NO_2^- concentration was generally constant after attaining a steady value of about 3 w/o, which is somewhat less than the value for the $NO_3^- = NO_2^- + 1/2\ O_2$ equilibrium in air at the maximum temperature of the loop, based on a value for the equilibrium constant of 18.5 $atm^{-1/2}$ [14]. The $CO_3^=$ concentration appears to increase about linearly with time from the initial value.

Results

The information obtained concerning the chemical and physical processes which affect 304SS in molten nitrates were derived from an analysis of the extent and composition of surface oxidation products, weight changes, microstructural changes and accumulation of metallic elements in the salt. The results which follow are categorized according to these general classifications.

Corrosion Extent and Morphology

Molten nitrate salts are strong oxidizing agents, although the identity of the active oxidant species is uncertain [15]. In this study, all the corrosion products identified were oxides. Their structures will be discussed shortly, but initially, the extent of scaling is of greatest interest since it indicates directly the suitability of a material for a particular application.

An Arrhenius-type plot of total oxide scale thicknesses measured on 304SS coupons immersed at various temperatures is shown in Figure 2, where the error bars indicate observed variations in scale thicknesses on each specimen and uncertainties in the temperature measurements. The plot indicates that approximately 12 μm (0.5 mil) of scaling occurred after 4200 hours at 595°C. Extrapolating linearly, about 25 μm (1 mil) of scaling would be expected after one year of isothermal immersion in molten nitrate salt. At temperatures below 550°C, the corrosion rate decreases to insignificant values.

The log (oxide thickness) versus 1/T data does not appear to be linear for the range of temperature shown. The temperature sensitivity of the aggregate oxidation rate increases as the temperature increases from 550°C. This increase in the activation energy of the corrosion process is probably related to the complex structure of the oxidation products formed, which are described below, and to a shift in the rate-controlling oxidation step.

Identification of oxidation products was emphasized for the coupons immersed at the highest temperatures where corrosion was most prominent. The general morphology of corroded specimens is indicated by the photomicrograph in Figure 3, which shows 304SS in cross-section after 4200 hours at 595°C. Three layers were differentiated by cathodic etching in aqueous Na_2CrO_4 [16].

The light gray layer in the middle was Fe_3O_4 (magnetite) which was identified by Debye-Scherrer x-ray diffraction patterns (XRD). In addition, scale fragments were observed to be magnetic. The layer between the Fe_3O_4 layer and the alloy was a mixed oxide spinel, $(Fe,Cr)_3O_4$, where Fe is the most abundant metallic element. Energy dispersive x-ray (EDX) spectra obtained on the scanning electron microscope indicated that the mixed oxide spinel was depleted in Cr relative to the Cr/Fe ratio in the alloy. The mixed oxide spinel was approximately the same thickness as the Fe_3O_4 layer.

The thin outer layer could not be identified unambigously. EDX analysis of polished cross-sections established only Fe and a minor amount of Ni as metallic constituents. EDX spectra of the surfaces of unmounted specimens indicated the presence of Mg, however, which is present as an impurity in the commercial grade salt used. Auger electron spectroscopy (AES) of surface layers on oxidized coupons demonstrated that Mg was present as illustrated in the AES scan in Figure 4. Since XRD did not indicate the presence of oxide phases, other than those discussed above, it seems likely that the outer layer was Fe_3O_4 which contained some double oxide of the type, $MgFe_2O_4$. The absence of a Mg signal in the EDX of polished specimens may be due to hydrolysis of the double oxide from prolonged aqueous contact during polishing [16].

The presence of Ni was indicated by EDX analysis in all three oxide layers. In addition, AES analysis of the oxide scale surface indicated the presence of Ni. The amount of Ni relative to Fe in each layer was somewhat less than the proportions in the alloy. It is probable that Ni was incorporated into the major oxide, Fe_3O_4, to yield a mixed spinel oxide of the type, $Ni_x\ Fe_{3-x}\ O_4$ [17], where the value of x has the upper limit of about 0.3 set by the alloy composition.

Weight Changes

Weight changes of coupons at various locations were determined as a function of time to supplement post-mortem metallographic analysis and were measured with the surface scales intact. Weight changes versus time for several 304SS coupons immersed at different temperatures are plotted in Figure 5.

The net weight changes observed at all temperatures were quite small although some general trends are discernable. The maximum positive weight changes were observed for coupons at a temperature less than the maximum temperature of the loop. Higher temperatures tended to cause a decrease in weight after long periods of time. In one specimen which was immersed at 595°C, reversals of the sign of weight changes versus time were observed. The interpretation of these weight change data will be considered in the discussion section to follow.

Weldments

Since salt containment structures will be assembled by welding, the corrosion behavior of weldments was studied briefly using autogenous weldments. Weight change vs. time curves for 304SS weldments, as a whole, behave similarily to the parent alloy. The weight changes recorded were quite small, not exceeding 0.5 mg/cm^2 after several thousand hours. The maximum weight gain did not occur at the highest temperature but rather at 540°C. At the highest temperature studied, 595°C, weight losses were observed.

Weldments were examined metallographically to determine if corrosion occurred preferentially in the fusion or heat-affected zones. As indicated by Table III, where data on the scale thicknesses above the three zones are collected, virtually the same amount of oxidation was found in the parent

alloy and fusion zone, while the heat-affected zone seemed to oxidize more. The structure of the oxide scale in the heat-affected zone has the same general appearance as that shown in Figure 3. No intergranular oxidation was observed in either the fusion or heat-affected zones.

Discussion

The data presented in the preceding sections show that alloy coupons display little or no weight gain despite the presence of surface oxide scales. For instance, at the highest temperatures where scaling is greatest (see Figure 2), weight changes are negligible (see Figure 5) compared to calculated weight gains of 1 mg/cm^2 for 7 μm of scale, based on an oxide density of 5.7 gm/cm^3. To account for the net weight changes, processes other than just oxidation must be considered.

Spalling of oxide layers is one possibility and could be important in view of the relatively small weight changes observed here. Although the scales on 304SS were found to be generally adherent from visual inspection, spalling of oxides at corners and edges of specimens could distort the results. Another weight loss mechanism which was observed was depletion of chromium from the alloy matrix. This phenomenon is discussed in greater detail in the following section.

Chromium Depletion

Chemical analyses of salt samples withdrawn periodically from the loop revealed that chromium was accumulating in the salt. A plot of Cr concentration as a function of time, in Figure 7, illustrates the accumulation of Cr. Although the absolute values of Cr concentration depend on the surface area/salt volume ratio of the loop, as well as physiochemical processes, the slope

of the data can shed some light on the controlling kinetic process. A least-squares fit of the data using a function of the type, log Cr = constant + n log t , yields a value for the slope, n, of 0.40. (Open circle points were not included in the regression analysis since these include contributions arising from the placement of additional coupons at 4200 hours.) This value is close to 0.5, which would arise if Cr loss from the alloy was controlled by diffusion in either the surface oxide layer or the alloy [18].

The identity of the Cr species in the melt has not been determined. However, due to the oxidizing nature of molten nitrates, it is likely that it is some type of chromate, either the Cr^{+3} oxidation state, CrO_4^{-5} or CrO_3^{-3}, or the Cr^{+6} oxidation state, CrO_4^{-2} or $Cr_2O_7^{-2}$. Although the trivalent form was found to oxidize to the hexavalent form, CrO_4^{-2}, at 250°C [19], a trivalent form was reported to consititute the majority of chromium when 316SS was immersed in molten HITEC for several thousand hours at 550°C [10].

The loss of Cr from the alloy was also evident from microstructural changes observed in cross-sectioned coupons. EDX analysis of the sublayer of alloy adjacent to the oxide scale demonstrated that this region was depleted in Cr compared to the initial bulk concentration. The depleted subsurface alloy phase is identified in the photomicrograph in Figure 8 after suitable etching. As noted previously, the oxide scales also contained proportionately more Fe than Cr relative to the alloy. It is therefore clear that the alloy experienced a net loss of Cr which has accumulated as a soluble ion in the melt.

Mass Transfer

As discussed in the previous section, the concentration of Cr in the salt increased continuously. If an asymptotic value of Cr concentration had been

reached, it would imply that Cr precipitated in the cold part of the loop, balancing inputs arising from depletion in the hot section. Furthermore, Fe and Ni were not detected at levels significantly above a few ppm, the sensitivity limits of the atomic absorption spectrometer. Thus, any mass transfer process involving Fe or Ni would be extremely slow. Finally, given the relatively low coupon weight losses observed here, it is evident that thermal gradient mass transfer will not be significant.

An AES examination of the surface of a tube section at the 350°C part of the loop revealed no enrichment of the alloying elements. AES did indicate that the thin ($\leq$ 1 μm) deposit observed was primarily Mg, Ca, Si, C and O as shown in the spectra in Figure 9. The elements in the deposit derive primarily from impurities in the salt except for O and C, which may be provided by the atmosphere. The deposit appears to be a mixture of alkaline earth silicates and carbonates which are insoluble in the melt. Deposits of this type appear to present no operational problems since they are limited by the low initial concentrations of these elements in the salt.

Practical Considerations

The results described above must be interpreted with respect to several factors to develop a clearer idea of how materials will perform in operating systems. Some of these factors are discussed briefly in this section, including the effects of surface finish, thermal cycling and the atmosphere in contact with the salt.

Metallographic analysis of sections of tubing removed from the loop provided information on the effect of surface finish on corrosion. The tubing was used in the as-received condition in contrast to the 180 grit polish given coupons. The amount of scaling of several sections from the heated leg is given in Table IV. These data can be compared directly with the amount of

scaling observed on polished coupons given in Figure 2. The data are not sufficiently precise to support the conclusion that a parabolic rate law is valid for extrapolating scaling rates found on polished coupons, at 4200 hours, to yield rates for as-received tubes, at 8500 hours. However, even if corrosion kinetics were linear, Table IV indicates that tubes did not differ drastically from polished surfaces and establishes a worst-case scaling rate of about 1 mil/yr.

A photomicrograph of a cross-sectioned tube removed from the part of the loop at 600°C appears in Figure 8 and can be compared with the scale morphology observed on polished coupons shown in Figure 3. The oxides composing the scale are the same as those on polished coupons, Fe_3O_4 and $(Fe,Cr)_3O_4$; but, the ordered layered structure seen in Figure 3 has been replaced by a relatively disordered structure. This feature is indicated by the vaguely defined boundary (revealed by an aqueous Na_2CrO_4 etch) between the light gray phase, Fe_3O_4, and the dark phase, $(Fe,Cr)_3O_4$, which is generally adjacent to the oxide-alloy interface.

The effect of thermal cycling, which is inherent in central solar receiver operation, on corrosion behavior will tend to increase rates as the protective oxide layers are fractured by thermal and growth stresses. This effect cannot be predicted reliably except by experiment. The scales observed on 304SS in this study were generally quite adherent. In particular, the adherence of scales formed on the inner diameter of tubes may benefit from the compressive stresses due to scale growth which tend to ensure contact of the scale and the tube.

Finally, it can be argued that the effect of operating the loop in a breathing mode, where the salt is not sealed from the atmosphere, does not create any special problems concerning corrosion behavior. Since CO_2

neutralizes oxide ions formed by decomposition of NO_3- or absorption of water vapor and thereby reduces alkalinity, CO_2 may reduce corrosion rates [7,8]. However, if it is necessary to prevent absorption of CO_2 by the melt, to avoid raising the melting point [20], exclusion of water vapor might also be necessary.

Conclusions

In molten $NaNO_3$-KNO_3, 304SS experienced about 25 μm/yr (1 mil/yr) of corrosion at 600°C (1110°F). Based on general corrosion considerations, these results imply that 304SS is a suitable containment material for long-term applications in central solar receivers or thermal energy storage. However, it is recognized that other factors, such as high temperature mechanical behavior, must be included when selecting alloys.

Corrosion occurred by formation of oxide scales which were multilayer structures composed of predominantly iron-rich rather than chromium-rich oxides. The temperature sensitivity of the oxidation rate increased as the temperature increased. Unpolished tube surfaces did not corrode at a significantly different rate than polished coupons although the scale morphology differed.

The formation of chromium-deficient oxides may be related to the tendency of chromium to dissolve in the melt. The concentration of chromium in the melt increased continuously with time according to parabolic kinetics. Chromium depletion resulted in a sub-surface alloy layer which was reduced in chromium.

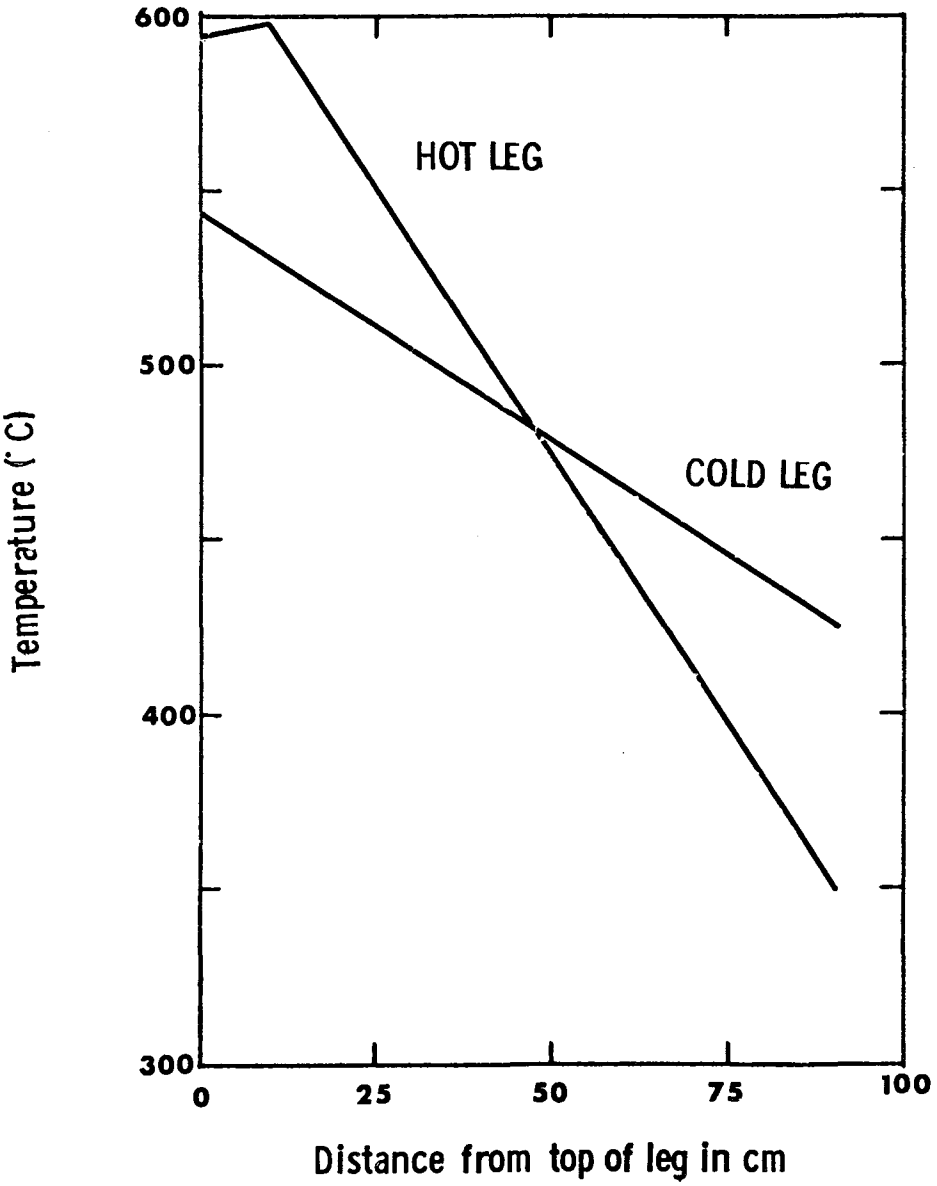

The Temperature Distribution in the Convection Loop

Figure 1

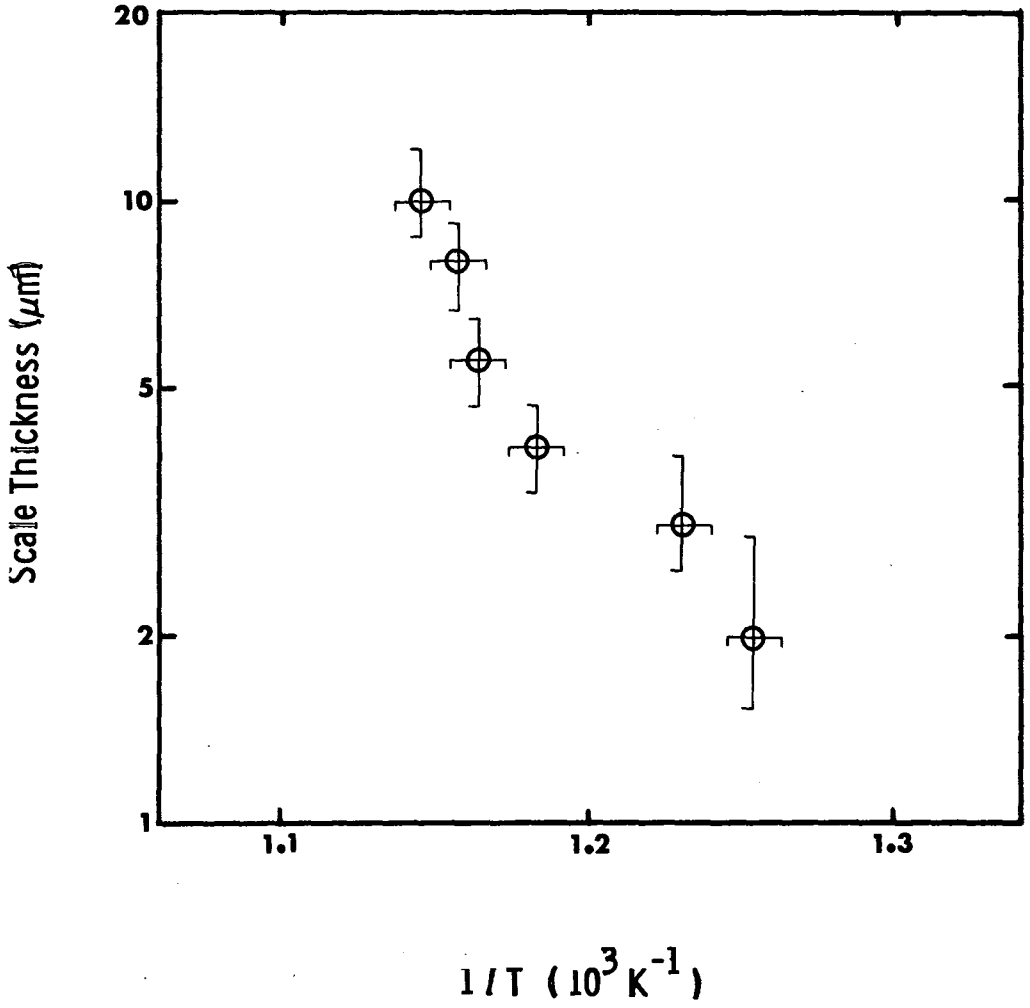

Extent of Scaling of 304SS after 4200 Hours in Molten $NaNO_3$-KNO_3

Figure 2

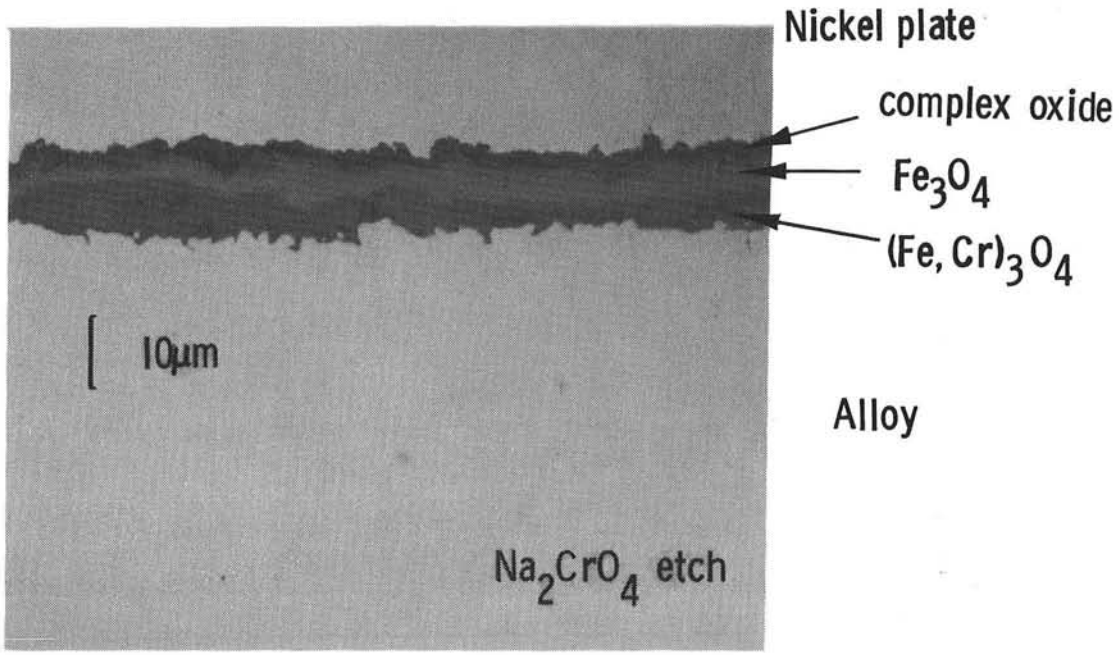

Oxide Structure on 304SS after 4200 Hours

Figure 3

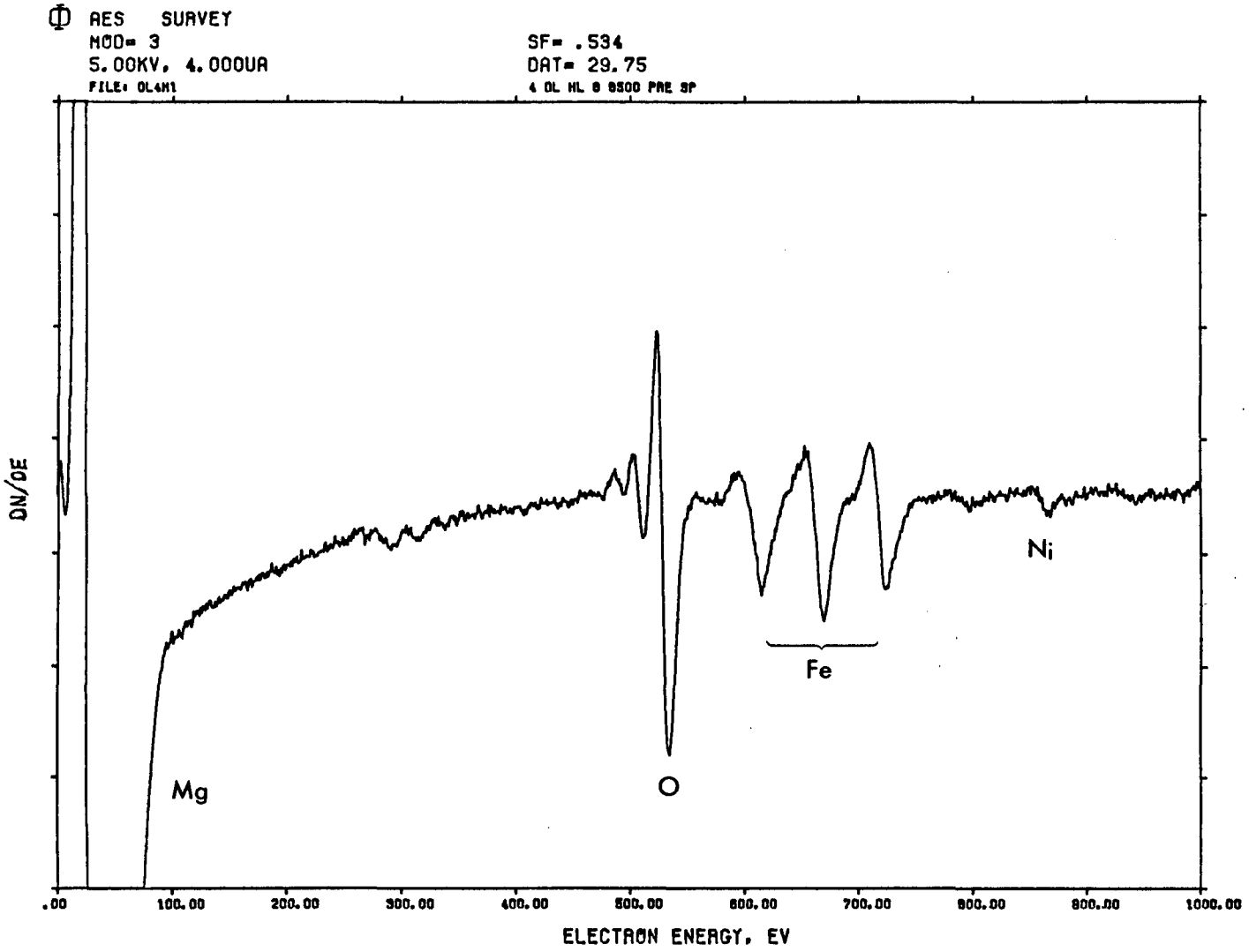

Auger Electron Spectrum of the Oxidized Surface of 304SS

Figure 4

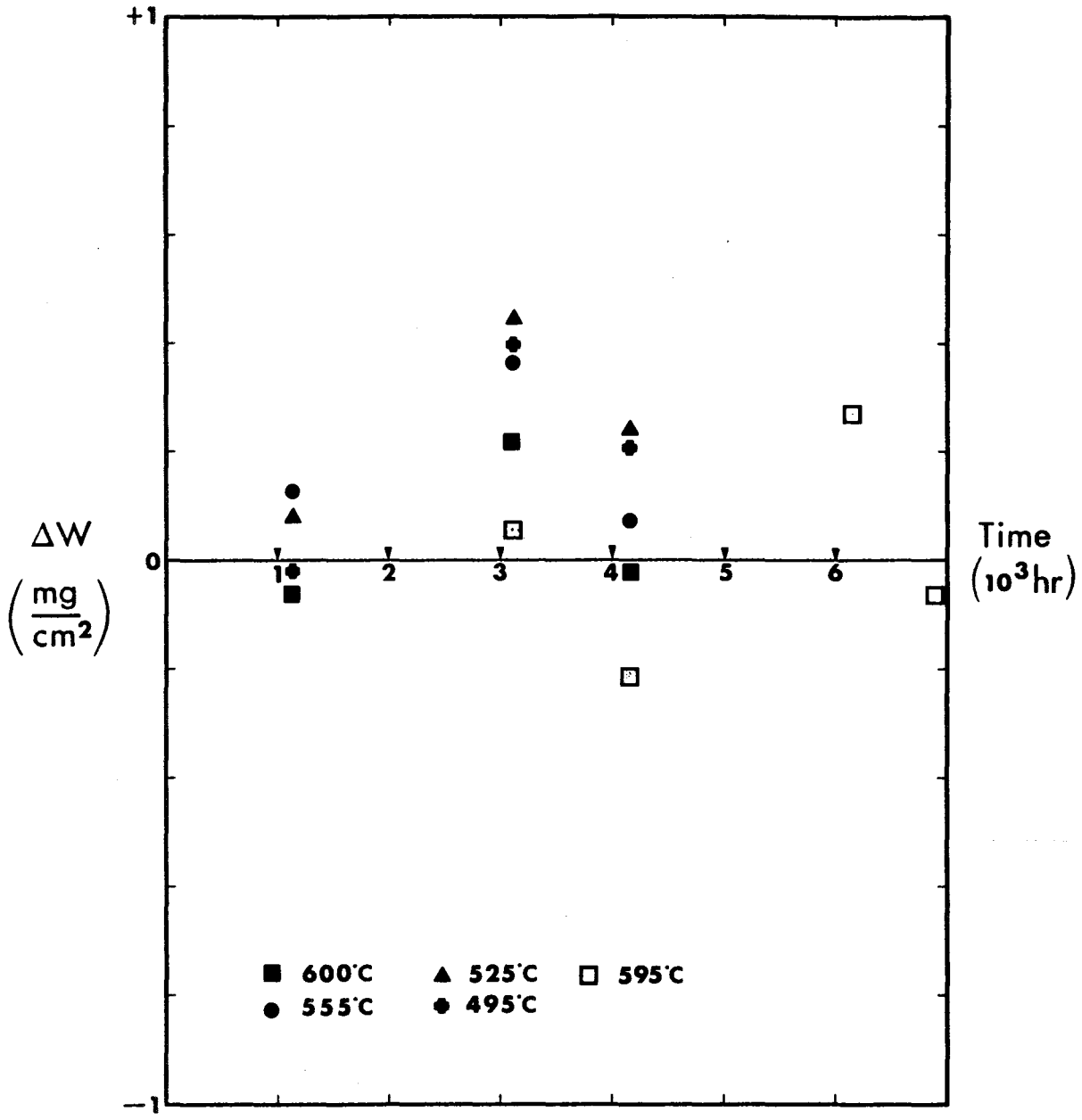

Weight Changes of 304SS vs. Time for Several Temperatures

Figure 5

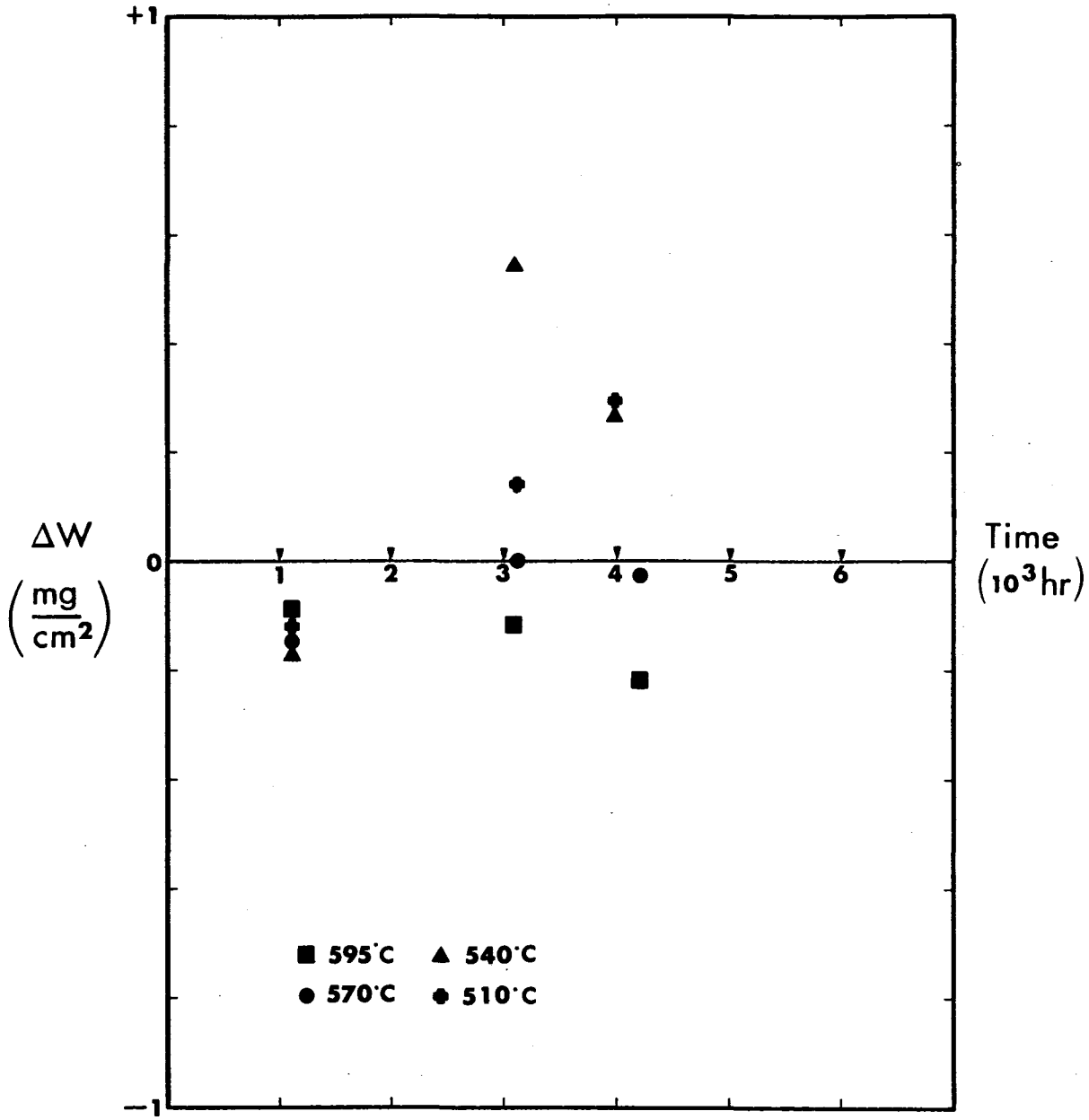

Weight Changes of 304SS Weldments vs. Time for Several Temperatures

Figure 6

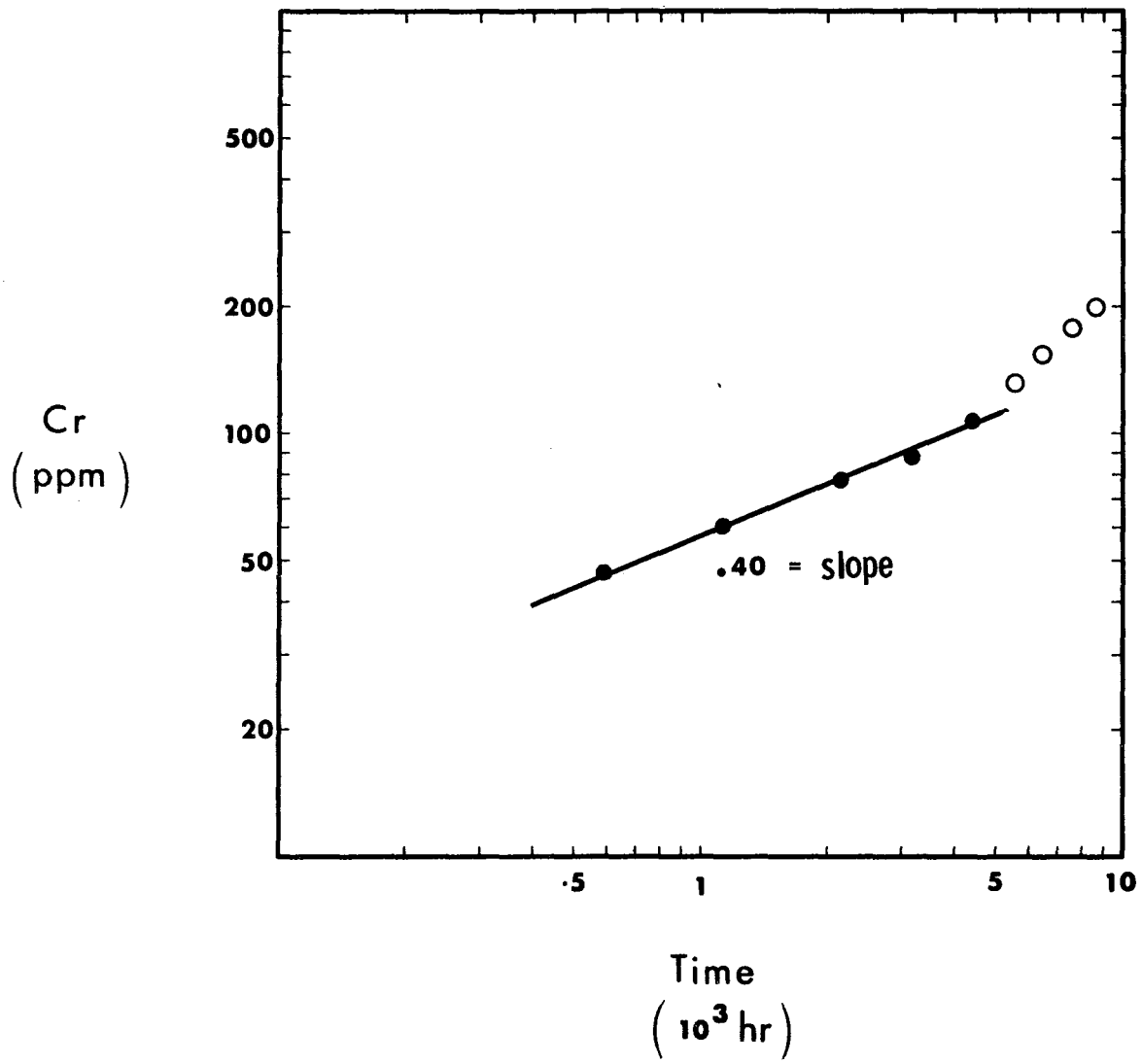

Chromium Concentration in the Melt as a Function of Time (log-log)

Figure 7

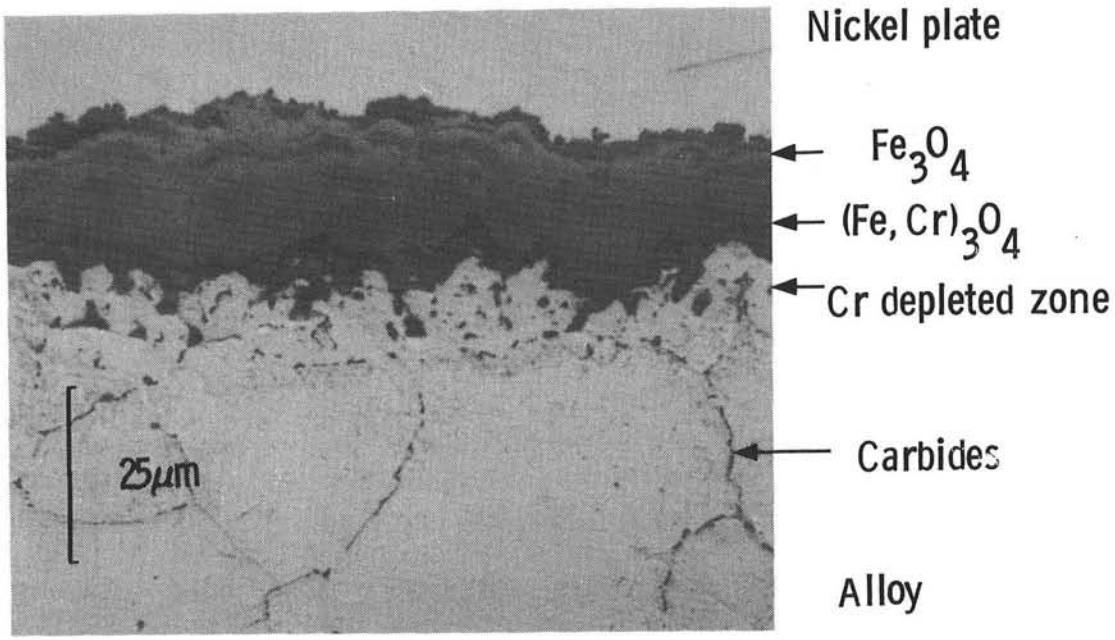

Etches : Na_2CrO_4 , Oxalic acid

Oxide Scale and Sub-Surface Alloy Structure of 304SS Tube Wall after 8500 Hours at 600°C

Figure 8

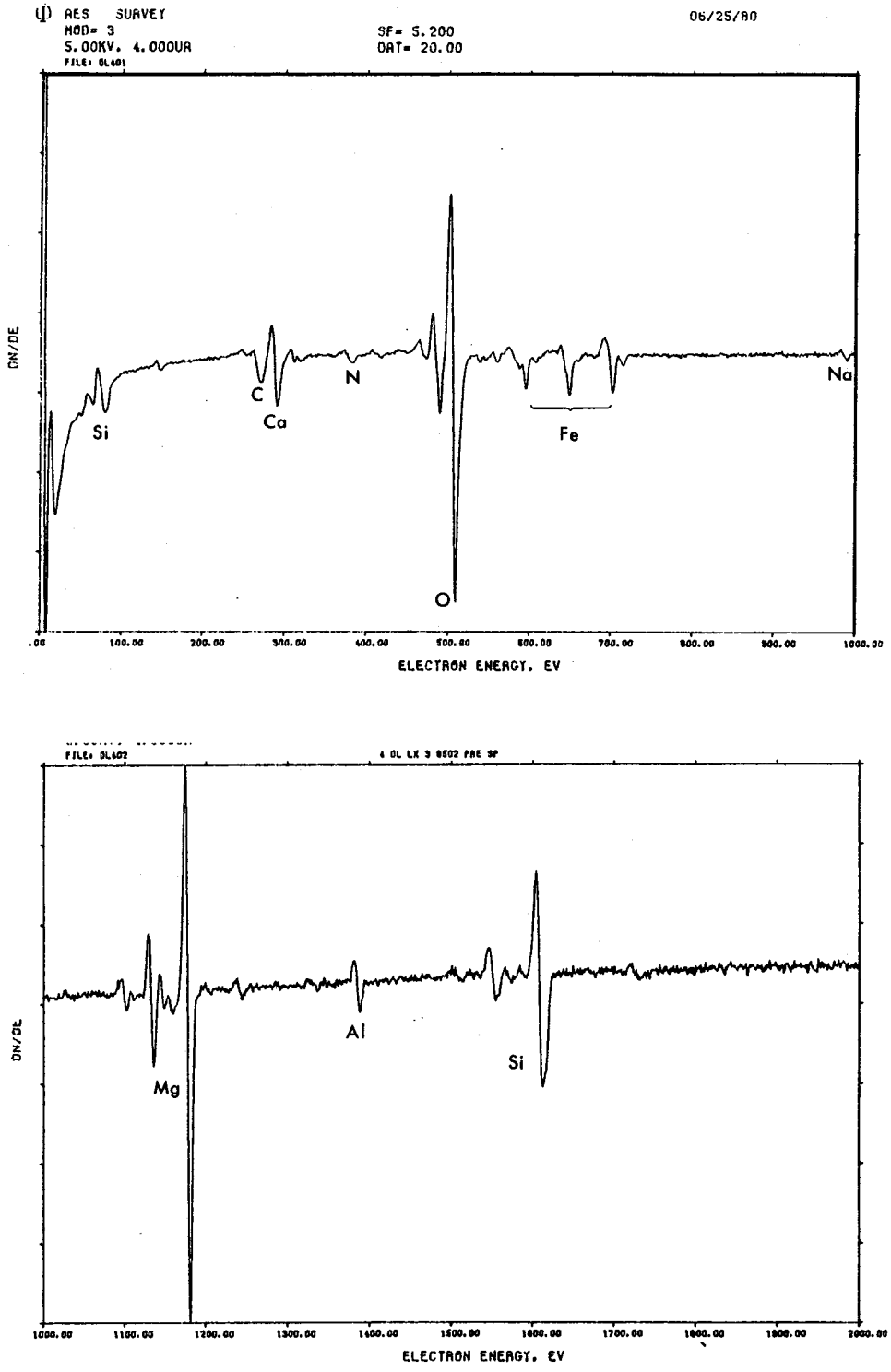

AES Analysis of Deposit on Tube Surface at 350°C after 8500 Hours

Figure 9

TABLE I

CHEMICAL COMPOSITIONS OF ALLOYS

Alloy	Coupons	Tubing
Cr	18-20	18.3
Ni	8-12	9.30
Mn	2 max	1.62
Si	1 max	0.52
Ti	-	-
C	0.08 max	0.06
other		Mo 0.06
		Cu 0.05

TABLE II

NITRITE AND CARBONATE CONTENT OF THE MELT DURING OPERATION OF THE LOOP

Time (hrs)	NO_2^- (w/o)	CO_3^- (w/o)
Start	0.08	0.19
574	2.6	0.27
1102	3.0	0.37
2045	3.1	0.33
4321	3.6	0.40
6361	3.0	0.42
8502	3.6	0.57

TABLE III

COMPARISON OF OXIDATION OF 304SS WELDMENT ZONES AFTER 4200 HOURS $NaNO_3$-KNO_3

Temperature (°C)	Total Scale Thickness* (μm)		
	Parent	Fusion	Heat-affected
595	7	9	11
590	9	9	12
540	4	5	7

*The uncertainties in the data are $\pm$ 1 μm at 540°C and $\pm$ 2 μm at the other temperatures.

TABLE IV

SCALING OF 304SS TUBING AFTER 8500 HOURS

Temperature (°C)	Scale Thickness	
	Mean (μm)	Range
600	16	9-25
575	11	6-15
550	9	5-13

REFERENCES

1. A. C. Skinrood, "High Temperature Solar Options for Electric Utilities and Users of Process Heat," Sandia National Laboratories, Report SAND80-8695, 1980.

2. L. N. Tallerico, "A Description and Assessment of Large Solar Power Systems Technology," Sandia National Laboratories, Report SAND79-8015, 1979.

3. J. R. Fried, Chem. Eng., 80, 89 May 28 (1973).

4. "Conceptual Design of Advanced Central Receiver Power Systems," Martin Marietta Corporation Report, Contract No. EG-77-C-03-1724, September 1978.

5. V. P. Burolla and J. J. Bartel, "The High Temperature Compatibility of Nitrate Salts, Granite Rock and Pelletized Iron Ore," Sandia National Laboratories, Report SAND79-8634, 1979.

6. M. D. Silverman and J. R. Engel, "Survey of Technology for Storage of Thermal Energy in Heat Transfer Salt," Oak Ridge National Laboratory, Report ORNL/TM-5682, 1977.

7. Y. I. Sorokin, and K. L. Tseitlin, Khim. Prom. 41 (1), 64 (1965).

8. M. Roche, Review Phys. Appl. 15, 895 (1980).

9. Kramer, C. M., W. H. Smyrl, and W. B. Estill, "Corrosion of Fe Alloys in Hitec at 823K," Sandia National Laboratories, Report SAND79-8256, 1979.

10. J. R. Keiser, J. H. DeVan and E. J. Lawrence, J. Nucl. Mater., 85, 275 (1979).

11. W. S. Winters, R. W. Bradshaw and F. W. Hart, "Design and Operation of Thermal Convection Loops for Corrosion Testing in Molten $NaNO_3$-KNO_3," Sandia National Laboratories, Report SAND80-8212, 1980.

12. H. R. Johnson, private communication, Sandia National Laboratories, Livermore, CA 1980.

13. D. E. Meeker and D. A. Nissen, private communication, Sandia National Laboratories, Livermore, CA 1980.

14. K. H. Stern, J. Phys. Chem. Ref. Data, 1, 747 (1972).

15. W. H. Smyrl, "Corrosion in Molten Salts Used for Solar Thermal Storage Applications," Sandia National Laboratories, Report SAND79-0246C, 1979.

16. M. H. Hurdus and L. Tomlinson, Br. Corros. J., 13, 158 (1978).

17. J. T. Foley, J. Electrochem. Soc., 109, 1202 (1962).

18. J. Crank, Mathematics of Diffusion, Oxford Univ. Press, London, 1967, p. 30ff.

19. B. J. Brough, D. H. Kerridge and S. A. Tariq, Inorg. Chem. Acta, 1, 267 (1967).

20. J. Alexander and S. G. Hindin, Ind. Eng. Chem., 39, 1044 (1947).

UNLIMITED RELEASE

INITIAL DISTRIBUTION:

USDOE (4)
Division of Thermal and Mechanical Energy Storage Systems
MS 6B025 Room 1G-100
Forrestal Building
Washington, D. C. 20585
Attn: J. H. Swisher
J. Gahimer
M. Gurevich
J. Brogan

USDOE
Albuquerque Operations Office
Special Programs Division
P. O. Box 5400
Albuquerque, NM 87115
Attn: D. Schueler

USDOE (2)
San Francisco Operations Office
1333 Broadway
Oakland, CA 94612
Attn: D. Elliott
L. Prince

USDOE (4)
Division of Solar Thermal Energy Systems
600 E Street N.W.
Room 419
Washington, D.C. 20585
Attn: G. W. Braun
M. U. Gutstein
J. E. Rannels
W. Auer
K. Cherian

Aerospace Corporation (2)
2350 El Segundo Blvd.
El Segundo, CA 90009
Attn: P. Mathur
L. R. Sitney

William D. Beverly
Boeing Engineering and Construction Co.
P. O. Box 3707
Seattle, WA 98124

Dr. C. A. Bolthrunis
Badger Energy, Inc.
One Broadway
Cambridge, MA 02142

William F. Clancey
Babcock and Wilcox Company
P. O. Box 351
Barberton, OH 44203

J. H. DeVan
Oak Ridge National Laboratory
Box X
Oak Ridge, TN 37830

James Elsner
General Electric
1 River Road
Schenectady, NY 12345

EPRI (2)
P. O. Box 10412
3412 Hillview Ave.
Palo Alto, CA 94303
Attn: J. Bigger
T. R. Schneider

Donald C. Erickson
Energy Concepts Co.
627 Ridgely
Annapolis, MD 21401

Dr. R. W. Foreman
Park Chemical Company
8074 Military Avenue
Detroit, MI 48204

General Atomic Co. (2)
P. O. Box 81608
San Diego, CA 92138
Attn: Thomas H. Van Hagan
Daniel L. Vrable

Skip Gross
MSA Research
Evans City, PA 16033

Steve P. Harnden
Arizona Public Service Company
P. O. Box 21666
Phoenix, AZ 85036

JPL (4)
4800 Oak Grove Dr.
Pasadena, CA 91103
Attn: V. Truscello
R. Manvi
J. Becker
W. Phillips

Robert M. N. Killen
United Engineers and Construction
Suite 300
3344 N. Torrey Pines CT.
La Jolla, CA 92137

Kenneth Ladd
Southwestern Public Service Co.
P. O. Box 1261
Amarillo, TX 79170

Robert L. Lessley
Bechtel
50 Beale
San Francisco, CA 94119

Donald J. Liffengren
Stearns-Roger
4500 S. Cherry Creek Drive
Denver, CO 80217

James P. Maddox
Biphase Energy Systems
2800 Airport Ave.
Santa Monica, CA 90405

Martin Marietta Corporation (4)
Box 179
Denver, CO 80201
Attn: Russell A. Chihoski
David W. Neiswander
Charles N. Bolton
Tom Tracey

McDonnell Douglas (3)
5301 Bolsa Ave.
Huntington Beach, CA 92647
Attn: George F. Greenwald
Donald L. Endicott
Russell T. Neher

Niven D. Morgan, Jr.
Vertac Chemical Corporation
Suite 241
3000 Knight Office Place
Shreveport, LA 71105

T. V. Narayanan
Foster Wheeler
12 Peach Tree Hill Road
Livingston, NJ 07039

John Neill
Advanced Energy Concepts
11722 Sorrento Valley Rd.
Suite I
San Diego, CA 92121

Soeren S. Nielsen
Gould, Inc.
40 Gould Center
Rolling Meadows, IL 60008

Bill Oberjohn
Babcock and Wilcox
Box 835
Alliance, OH 44601

Olin Corporation (3)
275 Winchester Ave.
New Haven, CT 06511
Attn: Louis C. Fiorucci
Stephen L. Goldstein
Joe K. Mensah

Olin Corporation (3)
120 Long Ridge Road
Stamford, CT 06904
Attn: Norman Christopher
Gerald A. Habib
Robert E. Smith

Dr. Robert A. Osteryoung
Department of Chemistry
State University of New York at Buffalo
Buffalo, NY 14214

Prof. Harald A. Oye
Institutt for uorganisk kjemi
Norges tekniske hogskole
Universitetet i Trondheim
N-7034 Trondheim - NTH, Norway

Pacific Gas and Electric (3)
3400 Crow Canyon Road
San Ramon, CA 94583
Attn: Helena T. Rowland
Harold E. Seielstand
Jay Raggio

Rockwell International
8900 De Soto Avenue
Canoga Park, CA 91304
Attn: Anarg Z. Frangos

Rockwell International/ESG
8900 De Soto Ave.
Canoga Park, CA 91304
Attn: Ted Johnson

Rockwell International/ETEC (2)
8900 De Soto Ave.
Canoga Park, CA 91304
Attn: Rick L. Howerton
Jerry B. Brukiewa

George H. Rowe
Combustion Engineering
1000 Prospect Hill Road
Windsor, CT 06095

SERI (8)
1536 Cole Blvd.
Golden, CO 80401
Attn: B. Butler
K. Touryan
B. P. Gupta
C. Wyman
P. A. Roberts
P. Russell
R. G. Nix
R. Ortiz (SERI Library)

Stuart A. Shiels
Westinghouse Electric Corporate
Advanced Reactors Division
Box 158
Madison, PA 15663

Richard D. Smith
Rocket Research Company
York Center
Redmond, WA 98052

Alan Snelson
ITT Research Institute
10 W 35 Street
Chicago, IL 60616

Donald J. Spellman
Gas Cooled Reactor Assoc.
3344 N. Torrey Pines Road
La Jolla, CA 92137

Pierre Spiteri
EDF
Les Renaidierz
Ecuelles
France

United Engineers and Construction
30 S. 17th Street
Philadelphia, PA 19103
Attn: John B. Mulligan

Robert J. Walter
Rocketdyne
6633 Canoga Ave.
Canoga Park, CA 91360

Sydney H. White
EIC Labs., Inc.
55 Chapel Street
Newton, MA 02158

Fred F. Witt
General Electric
3172 Porter Drive
Palo Alto, CA 94304

George Yenetchi
Solar Thermal Systems
Division of Exxon Enterprises Inc.
P. O. Box 592
Florham Park, NJ 07932

C. Winter, 400
A. Narath, 4000
J. H. Scott, 4700
G. E. Brandvold, 4710; Attn: B. W. Marshall, 4713
R. P. Stromberg, 4714
V. L. Dugan, 4720; Attn: J. V. Otts, 4721
J. F. Banas, 4722
J. A. Leonard, 4725
J. K. Galt, 5000
R. S. Claassen, 5800
R. G. Kepler, 5810
M. J. Davis, 5830; Attn: R. W. Rohde, 5832
N. J. Magnani, 5840; Attn: D. W. Schaefer, 5841

T. B. Cook, 8000
W. E. Alzheimer, 8120; Attn: R. J. Gallagher, 8124
A. N. Blackwell, 8200
B. F. Murphey, 8300
D. M. Schuster, 8310
R. W. Mar, 8313
R. W. Bradshaw, 8313 (24)
C. M. Kramer, 8313
A. S. Nagelberg, 8313
D. A. Nissen, 8313
J. C. Swearengen, 8316
S. H. Goods, 8316
R. Rinne, 8320; Attn: C. F. Melius, 8326
L. Gutierrez, 8400

R. Baroody, 8410
C. S. Selvage, 8420
C. M. Tapp, 8460
R. C. Wayne, 8450
P. J. Eicker, 8451
A. C. Skinrood, 8452
W. G. Wilson, 8453
R. W. Carling, 8453 (15)
L. G. Radosevich, 8453
Publications Division, 8265, for TIC (27)
Publications Division, 8265/Technical Library Processes Division, 3141
Technical Library Processes and Systems Division, 3141
Library and Security Classification Division, 8266 (3)